

A NEW MODEL FOR THE RADIO EMISSION FROM SN 1994I AND AN ASSOCIATED SEARCH FOR RADIO TRANSIENTS IN M51

KATE D. ALEXANDER, ALICIA M. SODERBERG, LAURA B. CHOMIUK¹
Harvard-Smithsonian Center for Astrophysics, 60 Garden Street, Cambridge, MA 02138
Submitted to the Astrophysical Journal

ABSTRACT

We present a new model for the radio emission from the Type Ic supernova 1994I and a search for additional transients in archival radio observations of the supernova. We find that the data are well fit by a standard synchrotron self-absorption model and estimate a pre-explosion mass loss rate of $\sim 2\text{--}5 \times 10^{-5} M_{\odot} \text{ yr}^{-1}$, which is consistent with a Wolf-Rayet progenitor. We also used a subset of the archival radio observations of SN 1994I to search for other radio transients in the supernova’s host galaxy, M51 (NGC 5194). This pilot study was conducted using archival data from the Very Large Array spanning a period of five months. Data were taken at a frequency of 4.9 GHz, with supplemental observations at other frequencies. Each epoch is 10-20 minutes in duration and epochs are irregularly spaced, enabling sensitivity to transients on timescales ranging from a few days to months. This image depth allows us to detect transients at the distance of M51 down to a luminosity of $\sim 4 \times 10^{25} \text{ erg s}^{-1} \text{ Hz}^{-1}$. We find no transient detections in 31 epochs of data, allowing us to place a 2σ upper limit of 17 deg^{-2} for the source density of transients above $500 \mu\text{Jy}$. This technique demonstrates the potential of high-cadence radio studies of local supernova host galaxies for revealing previously unknown radio transients.

Keywords: galaxies: individual (M51) — radio continuum: general — radio continuum: stars — supernovae: individual (SN 1994I)

1. INTRODUCTION

Twenty years after its discovery, SN 1994I retains its importance as the best-studied Type Ic supernova. Type Ic supernovae (SNe) are distinguished from other SNe in that they have no strong hydrogen or helium lines in their spectra. They are often grouped with Type Ib SNe (which contain helium but no hydrogen) because the two types show no significant differences in radio and X-ray emission. For the rest of this paper, we will refer to Ib and Ic SNe collectively as Type Ibc SNe. The progenitors of Type Ibc SNe have not yet been directly observed (Smartt 2009, Eldridge et al. 2013) but are commonly thought to be massive stars that have lost their outer envelopes of hydrogen gas prior to the time of explosion due to stellar winds or interaction with a companion. Two classes of progenitor candidates have been suggested: Wolf-Rayet stars (Woosley et al. 1995) and low mass helium stars with close binary companions undergoing mass transfer (Wellstein & Langer 1999; Yoon et al. 2010).

SN 1994I is located in the nearby spiral galaxy M51 (NGC 5194, the Whirlpool Galaxy) at a distance of $8.4 \pm 0.6 \text{ Mpc}$ (Feldmeier et al. 1997). Figure 1 shows its position within M51 at optical and radio wavelengths. SN 1994I was discovered on 1994 April 2 by four independent sets of observers (Puckett et al. 1994). Upper limits from optical observations of M51 taken prior to April 2 constrain the explosion date to no more than a few days before this, with the first detection of the SN found in an image from March 31.43 UT (Richmond et al.

1996). SN 1994I’s relative proximity allowed astronomers to obtain detailed observations spanning the electromagnetic spectrum (e.g. Filippenko et al. 1995; Richmond et al. 1996; Millard et al. 1999; Immler et al. 2002; Weiler et al. 2011). These observations have enabled better constraints on the progenitor models for Type Ibc SNe and still form a standard template to which observations of other Type Ic SNe are compared, as in the commonly-used SYNOW code (Fisher et al. 1997; Branch et al. 2007). This paper focuses on the radio observations of SN 1994I, first published in full by Weiler et al. (2011). Our analysis uses both their published flux values and an independent re-reduction of a subset of the radio observations publicly available on the VLA archive. The two reductions produce consistent results.

Radio observations of SNe provide a unique probe of the non-thermal synchrotron emission, which is generated as the SN blastwave passes through the circumstellar environment, shocking and accelerating particles ejected prior to the explosion by a wind from the progenitor star (Chevalier 1996). At a given radio frequency, the brightness of a radio SN follows a “bell-shaped” light curve, with emission rising to a peak and then subsiding over a period of several months. We find that the radio observations of SN 1994I are well-fit by a simple synchrotron self-absorption model (Chevalier & Fransson 2006), with no need for the additional complexities introduced in the model of Weiler et al. (2002). The advantage of our simpler model is that it allows us to derive interesting physical properties of the blastwave and explosion environment, including the blastwave radius R , the time-averaged velocity \bar{v} , the magnetic field strength B , and the pre-explosion mass loss rate \dot{M} . This model

kalexander@cfa.harvard.edu

¹ Department of Physics and Astronomy, Michigan State University, 567 Wilson Road, East Lansing, MI 48824

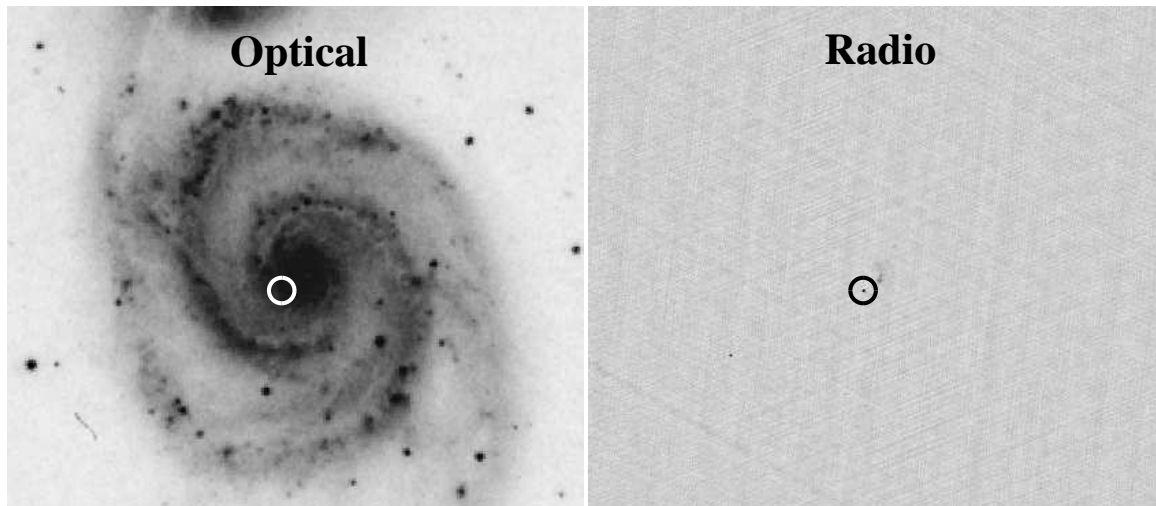


Figure 1. M51 at optical and radio wavelengths. The optical image is taken from the Digitized Sky Survey (DSS). The radio image is one of our re-reductions of archival VLA data and shows M51 in the C-band (4.9 GHz or 6 cm). This observation was taken when the VLA was in its B configuration. The circle in each image shows the position of SN 1994I. Each image is approximately 9 arcminutes by 9 arcminutes.

is discussed further in section 3.

In addition to studying SN 1994I itself, we reimaged a subset of the radio observations to search for other transient objects within the same field (section 4). A variety of radio transients have been observed and/or predicted, including radio supernovae (Weiler et al. 1986; Berger et al. 2003), radio pulsars (Hewish et al. 1968; Johnston & Romani 2003), afterglows associated with gamma ray bursts (Frail et al. 1997; Levinson et al. 2002), radio flares from brown dwarfs or extrasolar planets (Berger et al. 2001; Zarka 2007), X-ray binaries (Hansen & Lyutikov 2001), and tidal disruption events (Zauderer et al. 2013). Radio transients have the potential to exist at all radio wavelengths and can occur on timescales ranging from nanoseconds to years (Lazio et al. 2009). The exploration of this vast parameter space has only just begun (see Fender & Bell 2011 for a review). For the purpose of our survey, we consider a transient object to be an object which appears in one or more, but not all, consecutive epochs examined.

Collecting even moderately deep observations of large areas of the radio sky at a high enough resolution to detect most types of transients requires large amounts of observing time. Thus, most of the radio transients observed to date were either first discovered at other wavelengths or discovered serendipitously in the course of making other radio observations. Nevertheless, a number of blind imaging surveys have been undertaken. For instance, Levinson et al. (2002) and Gal-Yam et al. (2006) found a number of potential transient objects by comparing the FIRST and NVSS 1.4 GHz catalogs, covering an area of 2400 deg^2 to a sensitivity of 6 mJy, and Bannister et al. (2011) detected 15 transient objects in a 2776 deg^2 survey of the Southern sky at 843 MHz. More recently, Bell et al. (2014) found no transients in a 1430 deg^2 survey at 154 MHz, allowing them to set an upper limit of $7.5 \times 10^{-5} \text{ deg}^{-2}$ for the surface density of sources with flux densities $> 5.5 \text{ Jy}$. However, most radio imaging surveys are much smaller, often limited to single fields. Due to the nature of the data available, most single-field searches for radio transient objects have been limited to

calibration fields, as these are observed most regularly by radio telescopes. For instance, Bower et al. (2007) performed an extensive study of VLA data, using 944 epochs of a single field at two frequencies (5 and 8.4 GHz) taken over a 22-year period and finding 10 candidate transient objects with characteristic timescales between 7 days and 2 months. Additional work by Frail et al. (2012) eliminated some of these candidates and reduced the significance of others, emphasizing the importance of careful data reduction techniques and the availability of multi-wavelength data for followup observations. The nature of the remaining transients is still unknown.

While calibration fields are useful for transient surveys due to the fact that they are observed repeatedly, they are non-ideal from an astrophysical perspective because they are typically empty except for a single bright calibration source. While they are just as likely as any other field to contain very luminous transients at large distances, a field containing a nearby galaxy will likely have a higher concentration of nearby transient sources, allowing us to probe lower luminosity populations. This consideration makes a dataset of M51 observations a perfect candidate for a targeted radio transient search. Since the distance to M51 is known and we can assume that many of the transients we hope to observe will originate within the galaxy, this choice of field has the benefit of constraining the distance to the transients, which allows us to calculate their luminosity and thereby makes it easier to classify them and identify their progenitors. Furthermore, M51 has been a popular target for radio observations, particularly as several supernovae (SN 1994I, SN 2005cs, and SN 2011dh) have occurred within the galaxy in recent decades. As a result, the NRAO archive contains over 100 hours of public VLA observations of this galaxy at multiple wavelengths, spanning a period of nearly 30 years. We focused our transient search around observations of SN 1994I taken in the months following its discovery because they are closely spaced and of similar depth, facilitating easy comparisons between epochs. This pilot study verifies the feasibility of using archival VLA observations of nearby galaxies for tran-

sient searches and allows us to place an upper limit on the rate of radio transients in spiral galaxies. Our technique could easily be expanded to archival radio observations of other nearby galaxies, such as M82, where a similar SN monitoring program has already led to the serendipitous discovery of a transient thought to be an unusual microquasar (Joseph et al. 2011). SN 2008iz in M82 was also discovered serendipitously using radio observations originally collected for other purposes (Brunthaler et al. 2009a,b).

2. OBSERVATIONS AND ANALYSIS

2.1. Dataset

Our data comes from the Very Large Array (VLA) in Socorro, New Mexico. The VLA consists of 27 radio dishes, each 25 m in diameter, which are arranged along three radial arms in a Y pattern. The distances between the dishes can be adjusted, trading a longer baseline, which provides higher resolution, for a shorter baseline, which provides lower resolution and a higher sensitivity to diffuse emission. There are four configurations typically used: A, B, C, and D. The VLA changes from one configuration to the next every four months, passing through “intermediate” configurations (where one of the arms remains longer than the other two) as it does so. The intermediate configurations are denoted DnC, CnB, and BnA.

The flux density of the objects observed is typically determined by taking observations of a flux calibrator, a strong point source of known brightness. To account for atmospheric distortions, which can cause the phase offset between antennas to vary with time, a secondary phase calibrator is often also used. This is typically a nearby point source, observed alternately with the field of interest to keep track of changing conditions. In order to take full advantage of the data available, we have reduced data taken by multiple groups. Thus, the exact positioning of the array, the presence or absence of a flux calibrator, and the phase calibrator or calibrators used may all vary between epochs. Some epochs include scans of the flux calibrator 3C 286, but many rely solely on one or more phase calibrators. In these cases, the flux density is calibrated by using an estimate of the phase calibrator’s absolute flux density derived from a nearby epoch that did contain a flux calibrator. The most commonly used phase calibrator is J1418+546, which has an estimated flux density of approximately 0.97 Jy for the time period of our observations.

Intensive VLA monitoring of SN 1994I began a mere three days after its discovery, providing a rare opportunity to study the early properties of a Type Ibc SN. As observations taken with the VLA in C and D configurations were found to be dominated by diffuse emission from M51, which cannot be disentangled from point source emission using our simple reduction technique, we restricted our transient search to C-band (4.9 GHz) observations taken of M51 between 1994 April 5 and 1994 November 7. We independently reduced 31 epochs of data taken in the A, BnA, and B configurations and used them to generate maps of M51. Most of these observations were taken by the same group (PI Sramek) as part of the long-term monitoring of SN 1994I (Weiler et al. 2011). In addition to the C-band observations, these

epochs contain L-band (1.5 GHz), X-band (8.4 GHz), U-band (15.0 GHz), and K-band (22.5 GHz) data, allowing us to follow up transient candidates at other frequencies and obtain full radio spectra of any transients detected. All observations were conducted in dual polarization mode with a ten second dump time and have total integration times of 9-20 minutes. Each observation has a total bandwidth of 100 MHz, composed of two 50 MHz-wide IFs bracketing the central frequency for each band given above. The sensitivity of the VLA falls off as a 2D gaussian, so we can detect brighter transients in a larger area than dimmer transients. For 4.9 GHz data, the VLA has a half power beam width of ~ 9 arcminutes.

Light curves of SN 1994I at all five of the above frequencies have been previously published by Weiler et al. (2011). As a check on our reduction method, we reproduced the C-band light curve of SN 1994I using flux measurements extracted from our maps. The integrated flux of SN 1994I is plotted vs. days after the explosion of the SN in Figure 2 (using the explosion date assumed by Weiler et al. 2011, March 31.0 UT). In this figure, the red points are the original flux values reported in Weiler et al. (2011) and the blue points are the flux values we obtained from our independent reduction of the data. The two sets of flux values agree quite well, demonstrating the validity of our technique at 4.9 GHz.

2.2. Reduction Process

The data were reduced using the software package AIPS. After calibrating the data, we used the AIPS task IMAGR to generate cleaned images of the field. Figure 1 gives a typical output image and the same field at optical wavelengths. We sought to produce images covering the entire primary beam (that is, extending out to at least the half power beam width). No primary beam correction was applied. Since our resolution was dependent on the array configuration, as described above, the pixel size changed from one configuration to the next and the final size of images taken in different configurations ended up being slightly different. Ultimately, the area imaged ranged from 11 arcmin by 11 arcmin for the A configuration epochs to 13.6 arcmin by 13.6 arcmin for the B configuration epochs. Further details of the images used in the transient search are given in Table 1.

Once these cleaned images of the field were available, we used the AIPS task SAD (Search and Destroy) to detect all of the objects in each image. SAD searches for all peaks in an image down to a specified threshold level and fits two-dimensional Gaussians to these peaks. We ran two iterations, with flux cutoffs of 10σ and $5-6\sigma$. The transient detection threshold was set at either 5σ or 6σ , depending on the quality of the data in each image. The resulting mean central detection threshold of the images was $430 \mu\text{Jy}$. Assuming Gaussian noise, we predict no more than one false positive in our sample of 31 epochs for this cutoff. However, some calibrations were imperfect, due to non-ideal weather conditions and limited uv coverage, resulting in a number of detections generated by the resulting imaging defects. These were removed from our source catalogs for each image after a visual inspection of the data. The task JMFIT was then used to fit two-dimensional Gaussians to the brightest objects in each epoch, including SN 1994I and the galactic nucleus of M51. The SN 1994I fluxes were compared with the

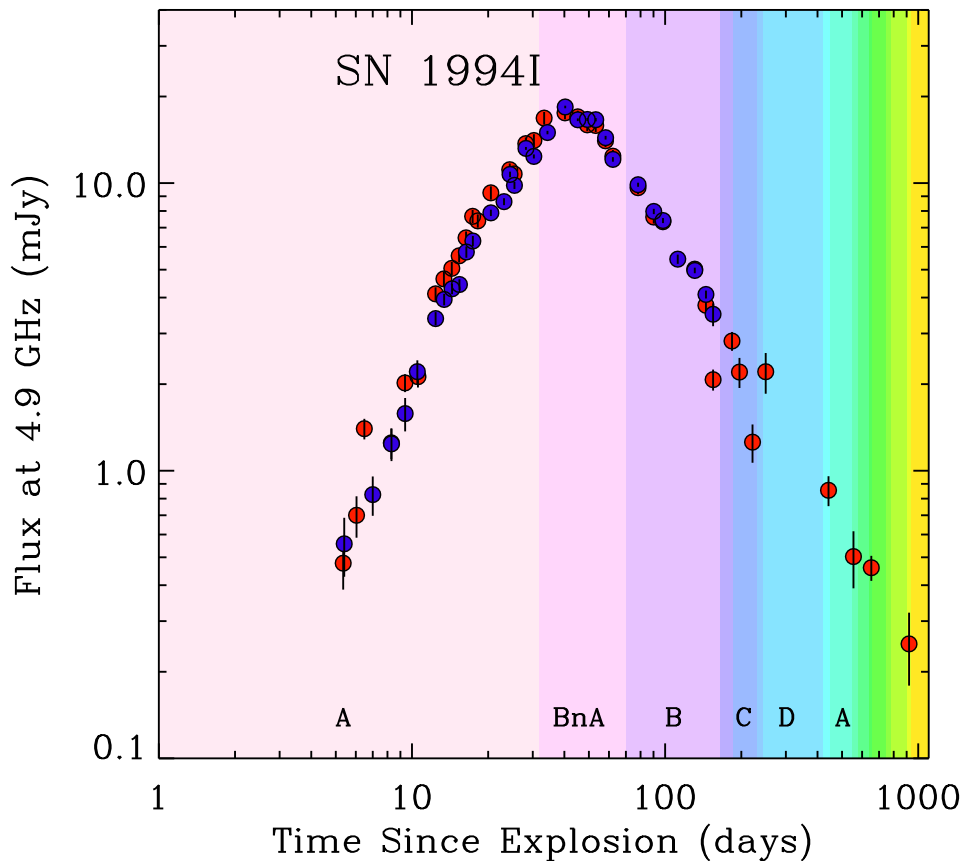


Figure 2. C-band (6 cm) observations of SN 1994I taken over a period of several years following its discovery. Our reduced data points are in blue, Weiler et al. (2011)’s data points are in red. Weiler et al. (2011)’s assumed explosion date of March 31.0 UT is used. The configuration of the VLA at the time of each observation is also shown.

Table 1
VLA Images Used in Transient Search

Configuration	Number of Epochs	Image Dimension (arcmin)	Clean Beam (arcsec)	Typical rms Noise ($\mu\text{Jy beam}^{-1}$)
A	18	11.0	0.35 x 0.27	90
BnA	6	11.4	1.2 x 0.48	60
B	7	13.6	1.4 x 1.1	100

Weiler et al. (2011) fluxes as mentioned above, providing a nice check on the accuracy of our technique. Further discussion of our transient search is deferred until section 4.

3. MODELING OF SN 1994I

In order to extract physical properties of SN 1994I and its progenitor star, we fit the observed flux values of the supernova with a model outlined in Chevalier (1998) and Chevalier & Fransson (2006). We note that this is simpler than the model developed in Weiler et al. (2002) and applied to the radio observations of SN 1994I by Weiler et al. (2011). In these papers, the authors generalize the simple Chevalier model to account for additional absorption due to distant HII between the SN and the observer, the effects of free-free absorption at early

times, and other complications. This leads to the introduction of several additional free parameters, which are determined from fits to the data. In the case of SN 1994I, Weiler et al. (2011) were forced to fix several of these parameters, as they could not be well-constrained by the data. Notably, they assume a homogeneous CSM with no clumps, just as our model does. Given that we obtain an equivalently good fit using the simple Chevalier model (our model has an overall $\chi^2 = 4.4$ per degree of freedom), we choose to use this model here for the additional physical parameter estimation that it allows.

In the Chevalier model that we use, the radio emission is explained as synchrotron emission from an interaction region between the supernova ejecta and material ejected from the progenitor star in a pre-explosion stellar wind. The rising part of the light curve is explained by syn-

Table 2

Physical Properties of SN 1994I. Based on fits to Weiler et al. (2011)'s reported fluxes assuming an explosion date of March 30.0 UT.

Age (days)	ν_{peak} (GHz)	F_{peak} (mJy)	R (10^{15} cm) ^a	\bar{v} ($c = 1$) ^b	B (G) ^c	E_ϵ (10^{45} erg) ^d	\dot{M} ($10^{-5} M_\odot \text{ yr}^{-1}$) ^e
10.125	22.5	14.80	2.39	0.0912	2.38	6.47	4.8
11.5 ^f	13.94	19.44	4.39	0.147	1.43	14.5	2.3
12.67	15.0	18.65	4.00	0.121	1.549	12.8	3.2
21.575	8.4	18.35	7.09	0.127	0.869	22.5	2.9
34.3	4.9	17.25	11.8	0.133	0.510	35.8	2.5
35.2 ^f	4.61	14.85	11.7	0.128	0.488	31.7	2.4
101.5	1.5	9.875	29.6	0.113	0.166	59.5	2.0
131.9 ^f	1.525	9.915	29.2	0.0854	0.168	58.8	4.1

^a Radius of blastwave in cm^b Time-averaged expansion velocity in units where $c = 1$ ^c Post-shock magnetic field strength in gauss^d Total internal energy of the blastwave in ergs^e Pre-explosion mass loss rate of the progenitor in solar masses per year, assuming $v_w \approx 1000$ km/s (typical for a Wolf-Rayet star).^f Parameters derived from the best-fit model for one of the spectra shown in Figure 4. Otherwise, parameters are derived from the best-fit model for one of the light curves shown in Figure 3.

chrotron self-absorption. At the peak, the synchrotron emission transitions from optically thick to optically thin. It then fades as the blastwave decelerates and the density of the circumstellar material decreases. The observed flux F_ν at radio frequency ν as a function of the time t elapsed since the explosion is given by (Chevalier 1998):

$$\frac{F_\nu(t)}{F_{\nu_p}(t_p)} = 1.582 \left(\frac{t}{t_p}\right)^a \left(\frac{\nu}{\nu_p}\right)^{5/2} \times \left\{ 1 - \exp \left[- \left(\frac{t}{t_p}\right)^{-(a+b)} \left(\frac{\nu}{\nu_p}\right)^{-(p+4)/2} \right] \right\}. \quad (1)$$

Here, F_{ν_p} is the peak flux at frequency ν_p , t_p is the time of peak flux at frequency ν_p , $a = 2m + 0.5$, and $b = (p+5-6m)/2$, where p is the energy spectral index of the relativistic electrons generating the synchrotron emission and m is related to the outer density profile of the SN ejecta. More specifically, the electrons are assumed to have a power-law distribution $N(E) = N_0 E^{-p}$ and $m = (n-3)/(n-2)$, where n is the power-law index of the SN outer density profile, $\rho \propto r^{-n}$. We use the ‘‘standard’’ model defined in Chevalier & Fransson (2006), which has $p = 3.0$ and $m = 0.88$. The time of peak flux t_p is, for our purposes, equivalent to the time at which the emission at frequency ν_p has an optical depth of unity.

We can use equation 1 to solve for F_{ν_p} and t_p for a time series of observations at a single frequency or for F_{ν_p} and ν_p for a set of radio observations taken at multiple frequencies at a specific time. The exquisite dataset compiled by Weiler et al. (2011) allows us to do both. Chevalier (1998) and Chevalier & Fransson (2006) then detail how to derive physical properties of the SN and progenitor from these numbers. Light curves of SN 1994I at five different frequencies are shown in Figure 3, along with the model given in equation 1. We determine the best-fit time of peak and peak flux of each light curve by minimizing a χ^2 value for a range of inputs for F_{ν_p} and t_p (and taking $\nu = \nu_p$ in equation 1). Initially, we followed Weiler et al. (2011) in assuming an explosion date

of March 31.0 UT. However, if we allow the explosion date to vary as well and reoptimize the χ^2 value for each frequency, we find that the best-fit explosion date ranges from March 28.9 UT (for the 4.9 GHz observations) to March 31.1 UT (for the 22.5 GHz observations). For our modeling, we therefore assume an explosion date of March 30.0 UT, the average of these five values. This explosion date has also been used by Millard et al. (1999). Both March 30.0 and March 31.0 are consistent with all known early observations of the supernova and our derived physical parameters are relatively insensitive to this change in the explosion date. These derived parameters are given in Table 2. Note that each light curve provides information about the SN system at the time of peak flux at the light curve frequency.

We also considered a full spectrum of radio observations of the SN at three different epochs (Figure 4), using the reported flux values of Weiler et al. (2011). The spectra span the frequency range 1.5-22.5 GHz and are all well-fit by the same synchrotron self-absorption model used to fit the SN 4.9 GHz light curve. The physical parameters derived from these fits are also given in Table 2. The results obtained for our second epoch, 1994 May 4, are consistent with those previously reported by Stockdale et al. (2005) (quoted in Chevalier & Fransson 2006). In general, the values derived from the spectra are in agreement with the values derived from the light curves, although there are a few minor discrepancies. This may be due to the smaller number of data points used to generate the fit for the spectra. Additionally, atmospheric effects become especially important at high frequencies and flux can become decorrelated if a calibrator is not observed every few minutes, making observations at these frequencies especially difficult. Note that the mass loss rate depends on the assumed pre-explosion wind speed of the progenitor, v_w . If we assume $v_w = 1000$ km s⁻¹, a typical wind speed for a Wolf-Rayet star, then we find a mass loss rate of $\dot{M} \sim 2.5 \times 10^{-5} M_\odot \text{ yr}^{-1}$, as quoted in Table 2. These values are consistent with expectations for Wolf-Rayet mass loss

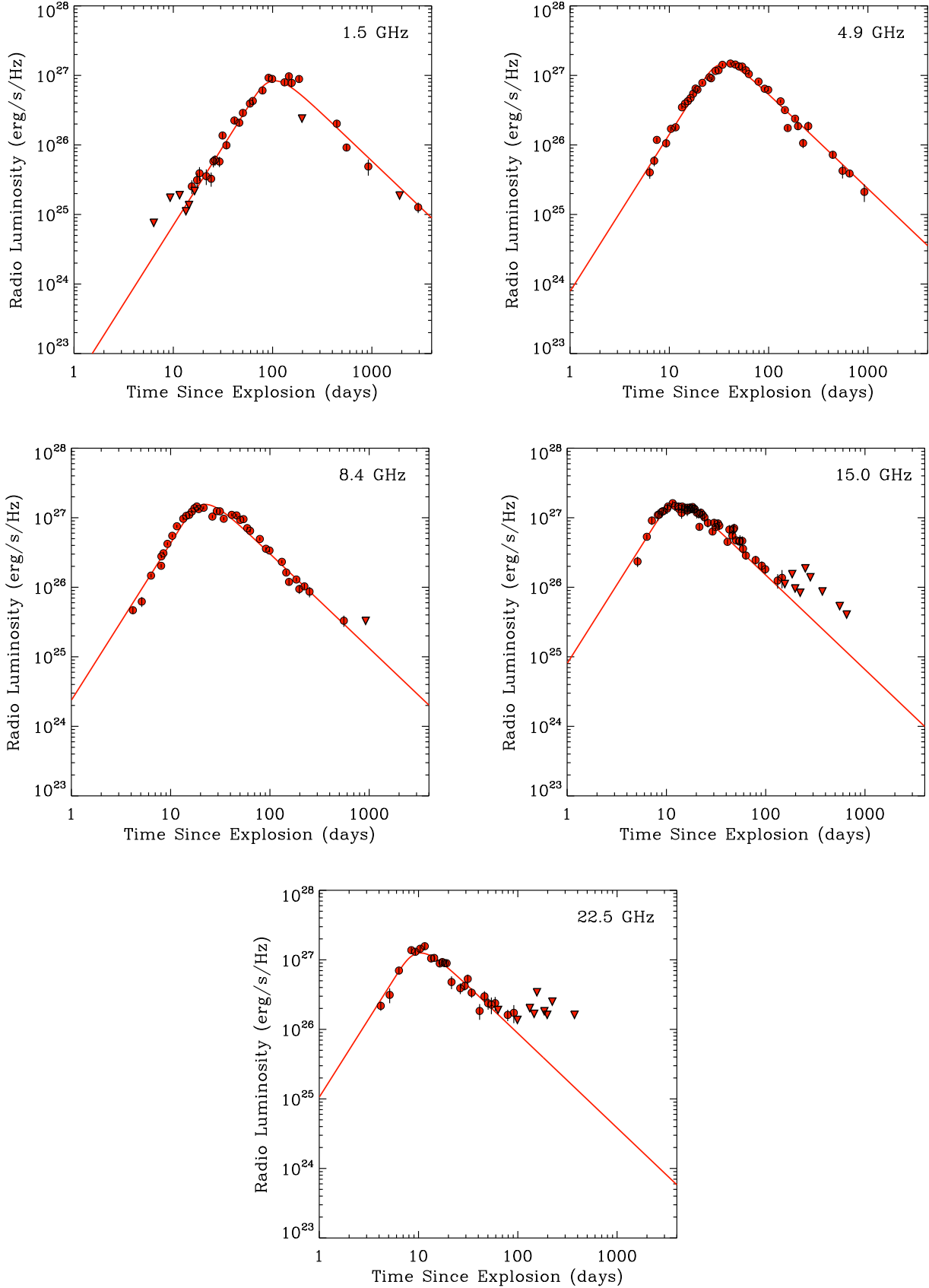


Figure 3. Light curves of SN 1994I at five radio frequencies. The red lines are the best-fit Chevalier & Fransson (2006) model for each frequency. The models assume an explosion date of March 30.0 UT. The red points are flux measurements taken from Weiler et al. (2011) and converted to luminosity assuming a distance of 8.4 Mpc for the SN. Triangles denote 3σ upper limits.

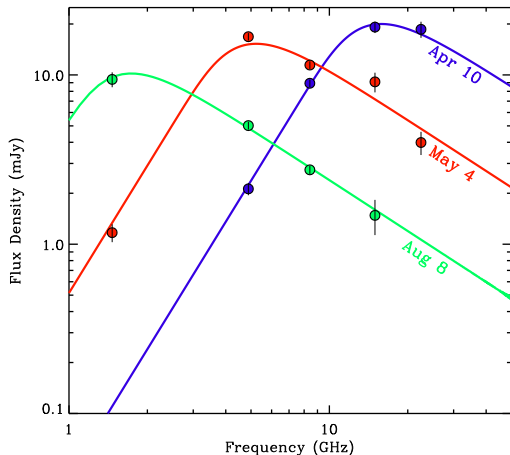


Figure 4. Spectra for SN 1994I at three different epochs in 1994 (dates indicated on graph). The data for each epoch is fit with a synchrotron self-absorption model with $p = 3$ (Chevalier & Fransson 2006). The flux values are taken from Weiler et al. (2011).

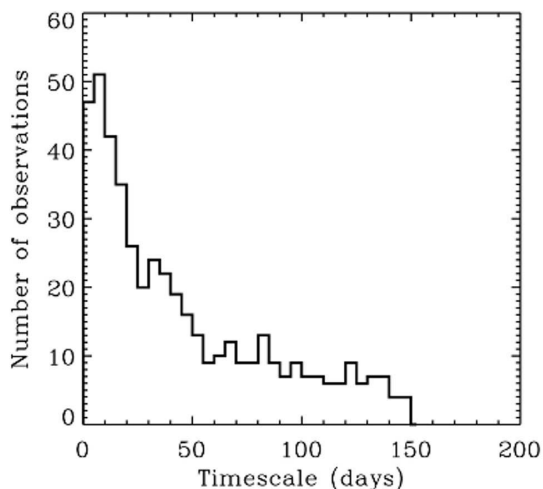


Figure 5. Histogram showing the time separations between all possible pairs of epochs used in our transient search. The number of observation pairs separated by a given amount of time is a rough estimate of our level of sensitivity to transients at that particular timescale. Our sensitivity peaks at a timescale of ~ 10 days and rapidly declines at longer timescales.

(Chevalier & Fransson 2006). Assuming a smaller wind speed of $v_w = 10 \text{ km s}^{-1}$ decreases this range to $\dot{M} \sim 2\text{-}5 \times 10^{-7} M_\odot \text{ yr}^{-1}$. Our estimate is much smaller than the mass loss rate $\dot{M} = 1 \times 10^{-5} (v_w/10 \text{ km s}^{-1}) M_\odot \text{ yr}^{-1}$ obtained by Immler et al. (2002) from X-ray observations of SN 1994I. Weiler et al. (2011) also computed mass loss rates based on the radio data that were lower than the X-ray estimate and suggest the discrepancy may be due to clumping of the CSM.

4. RADIO TRANSIENTS SEARCH

After confirming the quality of our maps by comparing our observed SN 1994I 4.9 GHz flux values to those reported by Weiler et al. (2011), we searched these maps for other transient objects. We used 31 epochs for our ra-

dio transient search, each 9-20 minutes in duration with typical sensitivities of $60\text{-}100 \mu\text{Jy beam}^{-1}$ rms. The detection threshold was set at 5σ or 6σ , depending on image quality. The observations are logarithmically spaced, with a time difference of 1-10 days between consecutive epochs. The non-constant spacing between epochs makes us varyingly sensitive to transients on different characteristic timescales, ranging from 10 minutes to 5 months. However, since we have many pairs of observations separated by timescales of a few days, and only one pair separated by 5 months, we note that our sensitivity to longer-duration transients is low (see Figure 5). In particular, we might be expected to miss most transients occurring at timescales longer than about 10 days (the maximum separation between two consecutive epochs).

We generated a list of radio sources in each epoch using SAD, as described in section 2.2. SN 1994I was detected in all of our epochs, as was emission from the nucleus of M51. Three other bright sources were also regularly detected, and therefore classified as non-transients. The positions and fluxes of these five objects are given in Table 3. In addition to these five steady sources, we initially detected 99 candidate transient objects. Each of these objects was only detected in an individual epoch, constraining the characteristic timescales of the candidates to between 9 minutes (the minimum epoch duration) and 10 days (the maximum separation between consecutive epochs). A significant fraction of our candidate list was discarded as imaging defects based on a visual inspection of the data, leaving us with a list of 30 possible transients. This list was compared with the catalog of radio sources in M51 compiled by Maddox et al. (2007), which was created using much deeper radio observations of M51 at 1.425 GHz and 4.860 GHz. The total on-source integration time for their 4.86 GHz data was 22.5 hours and their images reached a sensitivity of $11.7 \mu\text{Jy beam}^{-1}$ rms. Two of our transient candidates were also detected by Maddox et al., who found them to have flux densities of $264 \pm 14 \mu\text{Jy beam}^{-1}$ and $443 \pm 12 \mu\text{Jy beam}^{-1}$ respectively (Maddox et al. 2007 Table 2, sources 3 and 97). We obtained flux densities of $341 \pm 61 \mu\text{Jy beam}^{-1}$ for source 3 and $378 \pm 57 \mu\text{Jy beam}^{-1}$ for source 97. Both of these objects were only detected on 1994 August 8, which was the deepest observation collected when the VLA was in B configuration. The fact that we only detected these two objects in a single epoch of data may be because their fluxes are below our average sensitivity limit, but it may also be evidence of variability.

We further refined our list of transient candidates by selective reimagining of epochs containing one or more candidates. The observations for each epoch contain two IFs and two polarizations, so we reimaged the epochs containing one or more candidates, taking each IF and each Stokes parameter separately. Objects not detected in all four of the resulting images were discarded as false detections, eliminating all but four candidates. All of the epochs in our transient search also contain data taken at four other radio frequencies, so we reduced some of this data to see if these remaining candidate transients were detected in these frequencies as well. We found that none of our four candidates were detected at 8.4 GHz or 1.5 GHz. As three of the candidates were marginal detections in a single epoch and the fourth was detected near

Table 3
Bright Radio Sources Detected in M51

Source	R.A. (J2000.0) ^a	Dec. (J2000.0) ^a	Integrated 4.9 GHz Flux Density (mJy) ^a	Notes
1	13 ^h 29 ^m 54 ^s .12	47°11′30″.33	variable	SN 1994I
2 ^b	13 ^h 29 ^m 52 ^s .71	47°11′42″.73	1.135 ± 0.011	Nucleus of M51 ^b
3	13 ^h 29 ^m 51 ^s .57	47°12′08″.01	0.946 ± 0.011	Maddox et al. source 37
4	13 ^h 30 ^m 05 ^s .13	47°10′35″.78	4.287 ± 0.014	Maddox et al. source 104
5 ^c	13 ^h 30 ^m 11 ^s .03	47°10′40″.75	0.482 ± 0.020	Maddox et al. source 107 (X-ray binary)

^a Taken from Maddox et al. (2007) (except for SN 1994I flux)

^b The main point-like component of the nuclear emission. The position and flux given are from Maddox et al. source 53, the component detected in the largest number of epochs. Some epochs, particularly in more compact configurations of the VLA, contain additional objects from the complicated diffuse emission near the galactic nucleus.

^c This object is only detected in a few of our epochs and may be variable. Our clearest detection is on 1994 August 8, when we find its integrated flux to be 0.44 ± 0.10 mJy.

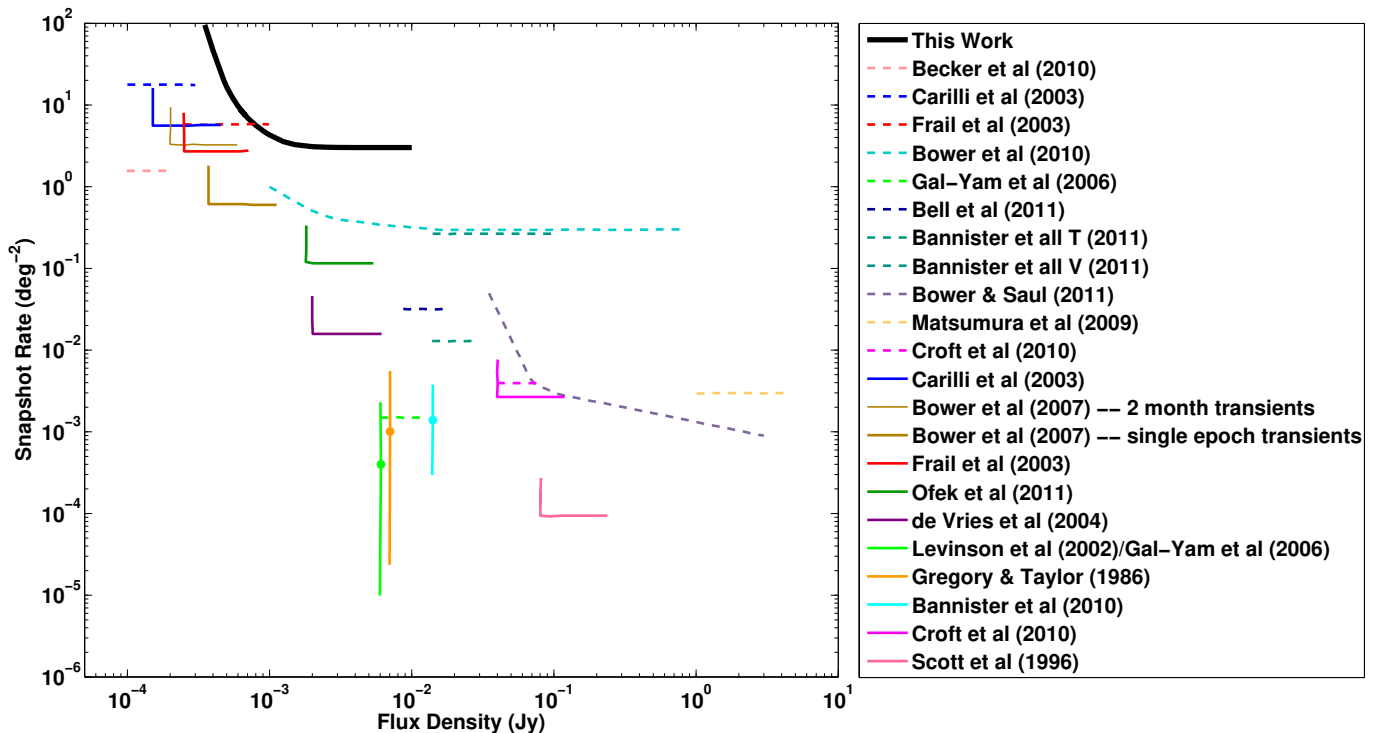


Figure 6. Summary of current radio transient snapshot rates and upper limits taken from Bell et al. (2011) (dashed lines) and Frail et al. (2012) (solid lines). Our 2σ upper limit, calculating using the procedure of Bell et al. (2011), is shown by the thick black line.

the location of the nucleus of M51 under poor observing conditions, we conclude that none of our candidates are real transients.

Our non-detection of transient objects in M51 allows us to place an upper limit on the transient population of this galaxy. Our mean central detection threshold of $430 \mu\text{Jy}$ corresponds to a luminosity of $3.7 \times 10^{25} \text{ erg s}^{-1} \text{ Hz}^{-1}$ at the distance of M51 (8.4 Mpc). This is comparable to the luminosity of Cassiopeia A, the most luminous SN remnant in the Milky Way (Reynoso & Goss 2002). The sensitivity of our images decreases with increasing radius, so to determine the observed rate of transients above a given flux density, we must first determine the area in each image within which we can detect objects of at least

the chosen brightness (see Bower et al. 2007). For the VLA, the half power radius at 4.9 GHz is equal to $4.5'$ (as determined above), and we compute the viable area in each image assuming a Gaussian decline in sensitivity. We then add up the viable areas from all of the images to obtain the total effective area N . The transient density (also called the snapshot rate) is the number of transients observed divided by N . Since we did not detect any transients, we follow the procedure of Bell et al. (2011) to determine a 2σ upper limit for the snapshot rate. For zero detections, they define the snapshot rate ρ using the equation

$$P(n) = e^{-\rho N}, \quad (2)$$

where $P(n) = 0.05$ corresponds to the 2σ upper limit with a confidence level of 95%. Thus, we can determine the upper limit for the snapshot rate of transients at any flux density by simply finding N for a given flux density cutoff and solving for ρ in Equation 2. For example, using this procedure, we find an upper limit of 17 deg^{-2} for the snapshot rate for transients of at least $500 \mu\text{Jy}$ (equivalent to a luminosity of $4.2 \times 10^{25} \text{ erg s}^{-1} \text{ Hz}^{-1}$ at the distance of M51). The current best estimates of the radio transient snapshot rate for various flux cutoffs are given in Figure 6, with our upper limit included as the solid black line (figure adapted from Bell et al. 2011). While this limit is less restrictive than other quoted works, it is also the only limit for a spatial region covering a nearby spiral galaxy. We therefore might expect the snapshot rate of our field to be higher than the snapshot rate in the empty spatial regions covered by the other surveys, making our upper limit significant. It is also possible to calculate an actual transient rate (the number of transients observed per deg^2 per year), but given the uncertainty in the characteristic timescales of the transients to which we would be sensitive (10 minutes to 10 days, as mentioned above), this is not particularly illuminating.

5. CONCLUSIONS

We presented a new model for the radio emission from SN 1994I, which fits the data well. While simpler than the model proposed by Weiler et al. (2011), our model allows us to calculate a number of interesting physical properties of the system, including the average expansion velocity of the blastwave as a function of time, the magnetic field strength, and the pre-explosion mass loss rate. The physical parameters of the system calculated from this model are consistent with a Wolf-Rayet progenitor for the SN. We also presented the results of a search for radio transients in M51 using archival 4.9 GHz VLA data, supplemented by observations at 1.5 GHz and 8.4 GHz. We detected no transients in 31 epochs spanning a five month period, setting an upper limit of 17 deg^{-2} on the transient density above $500 \mu\text{Jy}$. This is consistent with previously published upper limits and transient detection rates, and still allows for the transient rate of M51 to be higher than that observed in empty portions of the sky. Our pilot study shows that radio transient programs focused around a smaller field of view at high resolution are feasible with current facilities, particularly in regions with numerous existing archival observations. The recently upgraded VLA is a perfect instrument to conduct a larger high resolution radio transients search, as has already been suggested by Frail et al. (2012). The proposed VLA Sky Survey is expected to produce significant advances in radio transient science. The search for transients in nearby galaxies holds the potential to be especially scientifically interesting due to the higher probability of the presence of objects that could generate detectable transient radio emission, such as radio supernovae or X-ray binaries.

6. ACKNOWLEDGMENTS

Thanks to Jonathan McDowell and Marie Machacek for helpful comments on early drafts of this paper.

This work is supported in part by the National Science Foundation Research Experiences for Undergradu-

ates (REU) and Department of Defense Awards to Stimulate and Support Undergraduate Research Experiences (ASSURE) programs under Grant no. 0754568 and by the Smithsonian Institution.

The National Radio Astronomy Observatory is a facility of the National Science Foundation operated under cooperative agreement by Associated Universities, Inc.

This research has made use of SAOImage DS9, developed by Smithsonian Astrophysical Observatory.

REFERENCES

- Bannister, K. W., Murphy, T., Gaensler, B. M., Hunstead, R. W., & Chatterjee, S. 2011, *MNRAS*, 412, 634
- Bell, M. E., Fender, R. P., Swinbank, J., Miller-Jones, J. C. A., Law, C. J., Scheers, B., Spreew, H., Wise, M. W., Stappers, B. W., Wijers, R. A. M. J., Hessels, J. W. T., & Masters, J. 2011, *MNRAS*, 415, 2
- Bell, M. E., Murphy, T., Kaplan, D. L., Hancock, P., Gaensler, B. M., Banyer, J., Bannister, K., Trott, C., Hurley-Walker, N., Wayth, R. B., Macquart, J.-P., Arcus, W., Barnes, D., Bernardi, G., Bowman, J. D., Briggs, F., Bunton, J. D., Cappallo, R. J., Corey, B. E., Deshpande, A., deSouza, L., Emrich, D., Goeke, R., Greenhill, L. J., Hazelton, B. J., Herne, D., Hewitt, J. N., Johnston-Hollitt, M., Kasper, J. C., Kincaid, B. B., Koenig, R., Kratzenberg, E., Lonsdale, C. J., Lynch, M. J., McWhirter, S. R., Mitchell, D. A., Morales, M. F., Morgan, E., Oberoi, D., Ord, S. M., Pathikulangara, J., Prabu, T., Remillard, R. A., Rogers, A. E. E., Roshi, A., Salah, J. E., Sault, R. J., Udaya Shankar, N., Srivani, K. S., Stevens, J., Subrahmanyam, R., Tingay, S. J., Waterson, M., Webster, R. L., Whitney, A. R., Williams, A., Williams, C. L., & Wyithe, J. S. B. 2014, *MNRAS*, 438, 352
- Berger, E., Ball, S., Becker, K. M., Clarke, M., Frail, D. A., Fukuda, T. A., Hoffman, I. M., Mellon, R., Momjian, E., Murphy, N. W., Teng, S. H., Woodruff, T., Zauderer, B. A., & Zavala, R. T. 2001, *Nature*, 410, 338
- Berger, E., Kulkarni, S. R., Frail, D. A., & Soderberg, A. M. 2003, *ApJ*, 599, 408
- Bower, G. C., Saul, D., Bloom, J. S., Bolatto, A., Filippenko, A. V., Foley, R. J., & Perley, D. 2007, *ApJ*, 666, 346
- Branch, D., Parrent, J., Troxel, M. A., Casebeer, D., Jeffery, D. J., Baron, E., Ketchum, W., & Hall, N. L. Piersant, L. BurderiG. MattA. Tornambe & M. T. Menna, 342–349
- Brunthaler, A., Menten, K. M., Henkel, C., Reid, M. J., Bower, G. C., Falcke, H., & Green, D. W. E. 2009a, *Central Bureau Electronic Telegrams*, 1803, 1
- Brunthaler, A., Menten, K. M., Reid, M. J., Henkel, C., Bower, G. C., & Falcke, H. 2009b, *A&A*, 499, L17
- Chevalier, R. A. 1996, in *Astronomical Society of the Pacific Conference Series*, Vol. 93, *Radio Emission from the Stars and the Sun*, ed. A. R. Taylor & J. M. Paredes, 125–+
- Chevalier, R. A. 1998, *ApJ*, 499, 810
- Chevalier, R. A. & Fransson, C. 2006, *ApJ*, 651, 381
- Eldridge, J. J., Fraser, M., Smartt, S. J., Maund, J. R., & Crockett, R. M. 2013, *MNRAS*, 436, 774
- Feldmeier, J. J., Ciardullo, R., & Jacoby, G. H. 1997, *ApJ*, 479, 231
- Fender, R. P. & Bell, M. E. 2011, *Bulletin of the Astronomical Society of India*, 39, 315
- Filippenko, A. V., Barth, A. J., Matheson, T., Armus, L., Brown, M., Espey, B. R., Fan, X.-M., Goodrich, R. W., Ho, L. C., Junkkarinen, V. T., Koo, D. C., Lehnert, M. D., Martel, A. R., Mazzarella, J. M., Miller, J. S., Smith, G. H., Tytler, D., & Wirth, G. D. 1995, *ApJ*, 450, L11
- Fisher, A., Branch, D., Nugent, P., & Baron, E. 1997, *The Astrophysical Journal Letters*, 481, L89 [LINK]
- Frail, D. A., Kulkarni, S. R., Nicastro, L., Feroci, M., & Taylor, G. B. 1997, *Nature*, 389, 261
- Frail, D. A., Kulkarni, S. R., Ofek, E. O., Bower, G. C., & Nakar, E. 2012, *ApJ*, 747, 70
- Gal-Yam, A., Ofek, E. O., Poznanski, D., Levinson, A., Waxman, E., Frail, D. A., Soderberg, A. M., Nakar, E., Li, W., & Filippenko, A. V. 2006, *ApJ*, 639, 331
- Hansen, B. M. S. & Lyutikov, M. 2001, *MNRAS*, 322, 695

- Hewish, A., Bell, S. J., Pilkington, J. D. H., Scott, P. F., & Collins, R. A. 1968, *Nature*, 217, 709
- Immler, S., Wilson, A. S., & Terashima, Y. 2002, *ApJ*, 573, L27
- Johnston, S. & Romani, R. W. 2003, *ApJ*, 590, L95
- Joseph, T. D., Maccarone, T. J., & Fender, R. P. 2011, *MNRAS*, 415, L59
- Lazio, J., Bloom, J. S., Bower, G. C., Cordes, J., Croft, S., Hyman, S., Law, C., & McLaughlin, M. 2009, in *Astronomy*, Vol. 2010, *astro2010: The Astronomy and Astrophysics Decadal Survey*, 176–+
- Levinson, A., Ofek, E. O., Waxman, E., & Gal-Yam, A. 2002, *ApJ*, 576, 923
- Maddox, L. A., Cowan, J. J., Kilgard, R. E., Schinnerer, E., & Stockdale, C. J. 2007, *AJ*, 133, 2559
- Millard, J., Branch, D., Baron, E., Hatano, K., Fisher, A., Filippenko, A. V., Kirshner, R. P., Challis, P. M., Fransson, C., Panagia, N., Phillips, M. M., Sonneborn, G., Suntzeff, N. B., Wagoner, R. V., & Wheeler, J. C. 1999, *ApJ*, 527, 746
- Puckett, T., Armstrong, J., Johnson, W., Millar, D., Berry, R., Kushida, R., Richmond, M. W., Filippenko, A. V., Armus, L., & Mazzarella, J. M. 1994, *IAU Circ.*, 5961, 1
- Reynoso, E. M. & Goss, W. M. 2002, *ApJ*, 575, 871
- Richmond, M. W., van Dyk, S. D., Ho, W., Peng, C. Y., Paik, Y., Treffers, R. R., Filippenko, A. V., Bustamante-Donas, J., Moeller, M., Pawellek, C., Tartara, H., & Spence, M. 1996, *AJ*, 111, 327
- Smartt, S. J. 2009, *ARA&A*, 47, 63
- Stockdale, C. J., Sramek, R. A., Weiler, K. W., Van Dyk, S. D., Panagia, N., Montes, M. J., & Rupen, M. P. 2005, poster presented at IAU Colloq. 192, *Cosmic Explosions: On the 10th Anniversary of SN1993J*
- Weiler, K. W., Panagia, N., Montes, M. J., & Sramek, R. A. 2002, *ARA&A*, 40, 387
- Weiler, K. W., Panagia, N., Stockdale, C., Rupen, M., Sramek, R. A., & Williams, C. L. 2011, *ApJ*, 740, 79
- Weiler, K. W., Sramek, R. A., Panagia, N., van der Hulst, J. M., & Salvati, M. 1986, *ApJ*, 301, 790
- Wellstein, S. & Langer, N. 1999, *A&A*, 350, 148
- Woosley, S. E., Langer, N., & Weaver, T. A. 1995, *ApJ*, 448, 315
- Yoon, S.-C., Woosley, S. E., & Langer, N. 2010, *ApJ*, 725, 940
- Zarka, P. 2007, *Planet. Space Sci.*, 55, 598
- Zauderer, B. A., Berger, E., Margutti, R., Pooley, G. G., Sari, R., Soderberg, A. M., Brunthaler, A., & Bietenholz, M. F. 2013, *ApJ*, 767, 152